# Intranuclear dynamics of the Nup107-160 complex

Stéphanie Morchoisne-Bolhy[a], Marie-Claude Geoffroy[a], Imène B. Bouhlel[a,*], Annabelle Alves[a,b], Nicolas Audugé[a], Xavier Baudin[c], Kevin Van Bortle[d,†], Maureen A. Powers[d], and Valérie Doye[a]

[a]Institut Jacques Monod, CNRS UMR7592–Université Paris Diderot, Sorbonne Paris Cité, 75205 Paris, France; [b]Ecole Doctorale Gènes Génomes Cellules, Université Paris Sud, 91405 Orsay, France; [c]ImagoSeine Imaging Facility, Institut Jacques Monod, 75205 Paris, France; [d]Department of Cell Biology and Biochemistry, Cell and Developmental Biology Graduate Program, Emory University School of Medicine, Atlanta, GA 30322

**ABSTRACT** **Nup98 is a glycine-leucine-phenylalanine-glycine (GLFG) repeat–containing nucleoporin that, in addition to nuclear transport, contributes to multiple aspects of gene regulation. Previous studies revealed its dynamic localization within intranuclear structures known as GLFG bodies. Here we show that the mammalian Nup107-160 complex (Y-complex), a major scaffold module of the nuclear pore, together with its partner Elys, colocalizes with Nup98 in GLFG bodies. The frequency and size of GLFG bodies vary among HeLa sublines, and we find that an increased level of Nup98 is associated with the presence of bodies. Recruitment of the Y-complex and Elys into GLFG bodies requires the C-terminal domain of Nup98. During cell division, Y-Nup–containing GLFG bodies are disassembled in mitotic prophase, significantly ahead of nuclear pore disassembly. FRAP studies revealed that, unlike at nuclear pores, the Y-complex shuttles into and out of GLFG bodies. Finally, we show that within the nucleoplasm, a fraction of Nup107, a key component of the Y-complex, displays reduced mobility, suggesting interaction with other nuclear components. Together our data uncover a previously neglected intranuclear pool of the Y-complex that may underscore a yet-uncharacterized function of these nucleoporins inside the nucleus, even in cells that contain no detectable GLFG bodies.**

**Monitoring Editor**
Karsten Weis
ETH Zurich

Received: Feb 10, 2015
Revised: Apr 7, 2015
Accepted: Apr 14, 2015

## INTRODUCTION

Nuclear pore complexes (NPCs) are elaborate structures embedded in the nuclear envelope (NE) that provide the main route for bidirectional transport of a variety of molecules between the cytoplasm and the nucleus. They have a dual function as sieves that limit passive diffusion to small molecules less than ~40 kDa and as highly selective gates that facilitate the active import or export of large cargoes bearing specific targeting signals recognized by soluble nuclear transport receptors (reviewed in Wente and Rout, 2010; Floch *et al.*, 2014). NPCs are composed of ~30 different proteins called nucleoporins (Nups), each present in multiple copies due to the eightfold rotational symmetry of this structure, leading to an ~125-MDa assembly in vertebrates (reviewed in Floch *et al.*, 2014). Transmembrane Nups anchor the NPCs within the NE through their interaction with two core scaffold complexes: the central Nup93 complex, comprised of Nup53/Nup35, Nup93, Nup155, Nup188, and Nup205 in vertebrates (reviewed in Vollmer and Antonin, 2014), and the Nup107-160 complex, also termed the Y-complex because of its Y-shaped structure (reviewed in Gonzalez-Aguilera and Askjaer, 2012).

Y-complexes in vertebrates are composed of nine distinct subunits: Nup160/Nup120, Nup133, Nup107, Nup96, Nup85/Nup75, Nup43, Nup37, Seh1, and Sec13 (Loiodice *et al.*, 2004). They are symmetrically localized to both the cytoplasmic and nuclear faces of the NPCs; those on the nuclear side interact with the chromatin-binding nucleoporin partner Elys/MEL-28 (Belgareh *et al.*, 2001;

This article was published online ahead of print in MBoC in Press (http://www.molbiolcell.org/cgi/doi/10.1091/mbc.E15-02-0060) on April 22, 2015.

Present addresses: *CNRS UMR144–Institut Curie, 75248 Paris, France; †Department of Genetics, Stanford University, Stanford, CA 94305.

Address correspondence to: Valérie Doye (valerie.doye@ijm.fr).

Abbreviations used: aa, amino acid; Ab, antibodies; Act-D, actinomycin D; CNoBs, Crm1 nucleolar bodies; DAPI, 4′,6-diamidino-2-phenylindole; FG, phenylalanine-glycine; FRAP, fluorescence recovery after photobleaching; GFP, green fluorescent protein; GLFG, glycine-leucine-phenylalanine-glycine; LMB, leptomycin B; NE, nuclear envelope; NPC(s), nuclear pore complex(es); Nups, nucleoporins; qRT-PCR, quantitative reverse transcription PCR.

Rasala *et al.*, 2006; Bui *et al.*, 2013). Of importance, the interaction with Elys contributes to the recruitment of the Y-complex to chromatin at mitotic exit, a key step in the postmitotic reassembly of NPCs (Rasala *et al.*, 2006; Gillespie *et al.*, 2007). In addition, the entire Y-complex and Elys localize at kinetochores in mitosis and are required for proper cell division in mammalian cells (Loiodice *et al.*, 2004; Rasala *et al.*, 2006; reviewed in Wozniak *et al.*, 2010). Fluorescence recovery after photobleaching (FRAP) and turnover studies further revealed that the central structure of the NPC, notably the entire Y-complex, is composed of long-lived proteins that are very stably anchored within the NPCs in interphase, consistent with a function as a structural scaffold (Belgareh *et al.*, 2001; Rabut *et al.*, 2004; D'Angelo *et al.*, 2009; Savas *et al.*, 2012). In contrast, peripheral pore components exhibit a more dynamic behavior (Rabut *et al.*, 2004; D'Angelo *et al.*, 2009; Savas *et al.*, 2012).

Several of the peripheral Nups contain a domain formed of multiple phenylalanine-glycine (FG) motifs separated by spacer sequences. These unstructured and hydrophobic FG domains dynamically interact with nuclear transport receptors, giving to the FG-Nups a key function in active nucleocytoplasmic transport. In addition, certain FG domains associate via low-affinity, cohesive intramolecular and intermolecular interactions to form the permeability barrier of the pore (reviewed in Terry and Wente, 2009; Walde and Kehlenbach, 2010; Schmidt and Gorlich, 2015). Unique among vertebrate FG-Nups, Nup98 features a highly cohesive glycine-leucine-FG (GLFG) subtype of FG domain (Radu *et al.*, 1995; Powers *et al.*, 1995; Xu and Powers, 2013; Schmidt and Gorlich, 2015, and references therein). Significantly, chromosomal translocations involving Nup98 have been described in patients with leukemias, especially acute myeloid leukemia (reviewed in Gough *et al.*, 2011). Such translocations result in expression of fusion proteins that juxtapose the N-terminal GLFG/FG domain of Nup98 to the C-terminus of various partner proteins. Although still debated, the aberrant localization and function of the chimeras, as well as their interaction with endogenous Nup98, appear to contribute to leukemogenesis (reviewed in Gough *et al.*, 2011; Franks and Hetzer, 2013; see also Sarma and Yaseen, 2013; Salsi *et al.*, 2014).

Endogenous Nup98 is predominantly generated through autoproteolytic cleavage of a Nup98-Nup96 precursor that also generates Nup96, a subunit of the Y-complex. However, Nup98 can also be expressed independently of Nup96 from a differently spliced mRNA (Nup98-6kDa; Fontoura *et al.*, 1999; Rosenblum and Blobel, 1999; see later schemes in Figures 2C and 3A). After cleavage, the C-terminal autoproteolytic domain of Nup98 (amino acids [aa] 676–863) can interact with the N-terminal domain of Nup96 and Nup88 (Hodel *et al.*, 2002; Griffis *et al.*, 2003), thereby contributing to the anchorage of Nup98 to both sides of the NPC (Chatel *et al.*, 2012). Nup98 also directly interacts with Pom121 (Mitchell *et al.*, 2010), and binding of its N-terminal GLFG/FG repeat domain to Nup93 contributes to the dynamic association of Nup98 with NPCs (Xu and Powers, 2013).

The N-terminal GLFG/FG domain of Nup98 (aa 1–506) also serves as a docking site for several nuclear transport receptors, notably the nuclear protein export factor CRM1 (Oka *et al.*, 2010) and the RNA export factors TAP/NXF1 (Blevins *et al.*, 2003). Within this FG-containing region, a GLEBS domain allows Nup98 interaction with another RNA export factor, the nucleoporin Rae1/Gle2 (Pritchard *et al.*, 1999). Nup98 has been demonstrated to move on and off the nuclear pore in a transcription-dependent manner (Griffis *et al.*, 2002) and to contribute to multiple aspects of gene regulation. Via its GLFG/FG domain, Nup98 interacts with the histone-modifying enzyme CBP/p300 and the histone deacetylase 1 (Kasper *et al.*, 1999; Bai *et al.*, 2006). Nup98 also regulates posttranscriptional expression of defined p53 target genes (Singer *et al.*, 2012) and was recently shown to associate dynamically with the human genome, thereby regulating developmental gene expression programs (reviewed in Franks and Hetzer, 2013; see also Liang *et al.*, 2013).

Within the nucleus, Nup98 was previously shown to localize in distinct intranuclear bodies termed GLFG bodies. These bodies have been detected consistently in two cell lines (*Xenopus* XL177 and a HeLa subline termed HeLa-C; Griffis *et al.*, 2002; Xu and Powers, 2010), in *Xenopus* A6 cells, and in ~5% of HeLa CCL-2 cells (unpublished results). However, GLFG bodies can be induced in other cell lines upon Nup98 overexpression (Griffis *et al.*, 2002). Although the physiological significance of GLFG bodies remains elusive, previous studies addressing the dynamics of these structures have helped to elucidate several aspects of intranuclear Nup98 function, notably in mRNA and protein export (Griffis *et al.*, 2002; Oka *et al.*, 2010). However, besides the presence of the nuclear export factor CRM1 (Oka *et al.*, 2010), the composition of the GLFG bodies had not been previously investigated.

In the present study, we show that the Y-complex and its partner Elys dynamically colocalize with Nup98 and CRM1 into endogenous GLFG bodies present in specific HeLa sublines. FRAP studies further reveal the existence of a nucleoplasmic pool of Y-Nups outside of the nuclear bodies, suggesting a potential, as-yet-uncharacterized intranuclear function of these scaffold nucleoporins.

## RESULTS

### The Y-complex and Elys colocalize with Nup98 in intranuclear bodies

Nup107, a component of the Y-complex, has been characterized as a key structural component of the NPC during interphase (Belgareh *et al.*, 2001). However, anti-Nup107 antibodies also stained a few discrete intranuclear bodies, most frequently localized in the vicinity of the nucleoli, in ~20–30% of the cells from the HeLa subline we used (subsequently referred as HeLa-E; see *Materials and Methods*; Figure 1A). Unlike cytoplasmic annulate lamellae (membrane stacks containing NPC-like structures) or nuclear envelope invaginations (Fricker *et al.*, 1997), these Nup107-stained intranuclear bodies were not labeled by mAb414, which in mammalian cells recognizes several FG-Nups but not Nup98. Analysis of live or fixed HeLa-E cells stably expressing green fluorescent protein (GFP)–Nup107 or GFP-Nup43 (another constituent of the Y-complex) similarly revealed the presence of these two GFP-Nups within intranuclear bodies (Figure 1A; see later images in Figure 5A for live cells). Elys, a well-characterized Y-complex partner (Rasala *et al.*, 2006), was also enriched in these bodies (Figure 1A), a localization that mirrors the intranuclear staining recently observed for GFP-Elys (Bilokapic and Schwartz, 2013). These nuclear bodies were reminiscent of the previously described Nup98- and CRM1-containing GLFG bodies (Griffis *et al.*, 2002; Xu and Powers, 2010; Oka *et al.*, 2010). In support of this identification, we found Nup107, GFP-Nup43, and Elys colocalized with Nup98 and CRM1 in HeLa-E cells (Figure 1A).

These results prompted us to assess the localization of various Y-complex constituents (subsequently referred to as Y-Nups) in another HeLa subline, HeLa-C, in which a very high frequency of GLFG bodies was previously reported (Xu and Powers, 2010). In this cell line, >90% of the cells displayed intranuclear foci stained by Y-Nups (Nup107, Nup133, Nup96), Elys, and Nup98 (Figures 1B and 2A). In addition, transfection of GFP fusions in HeLa-C cells revealed that all tested Y-Nups and Elys were targeted to GLFG bodies (Figures 1C and 3D and Table 1). However, Y-Nups or Elys were not detectable in a subset of Nup98-containing GLFG bodies localized within the nucleoli (arrowheads in Figure 1C and Supplemental Figure S1A; unpublished data).

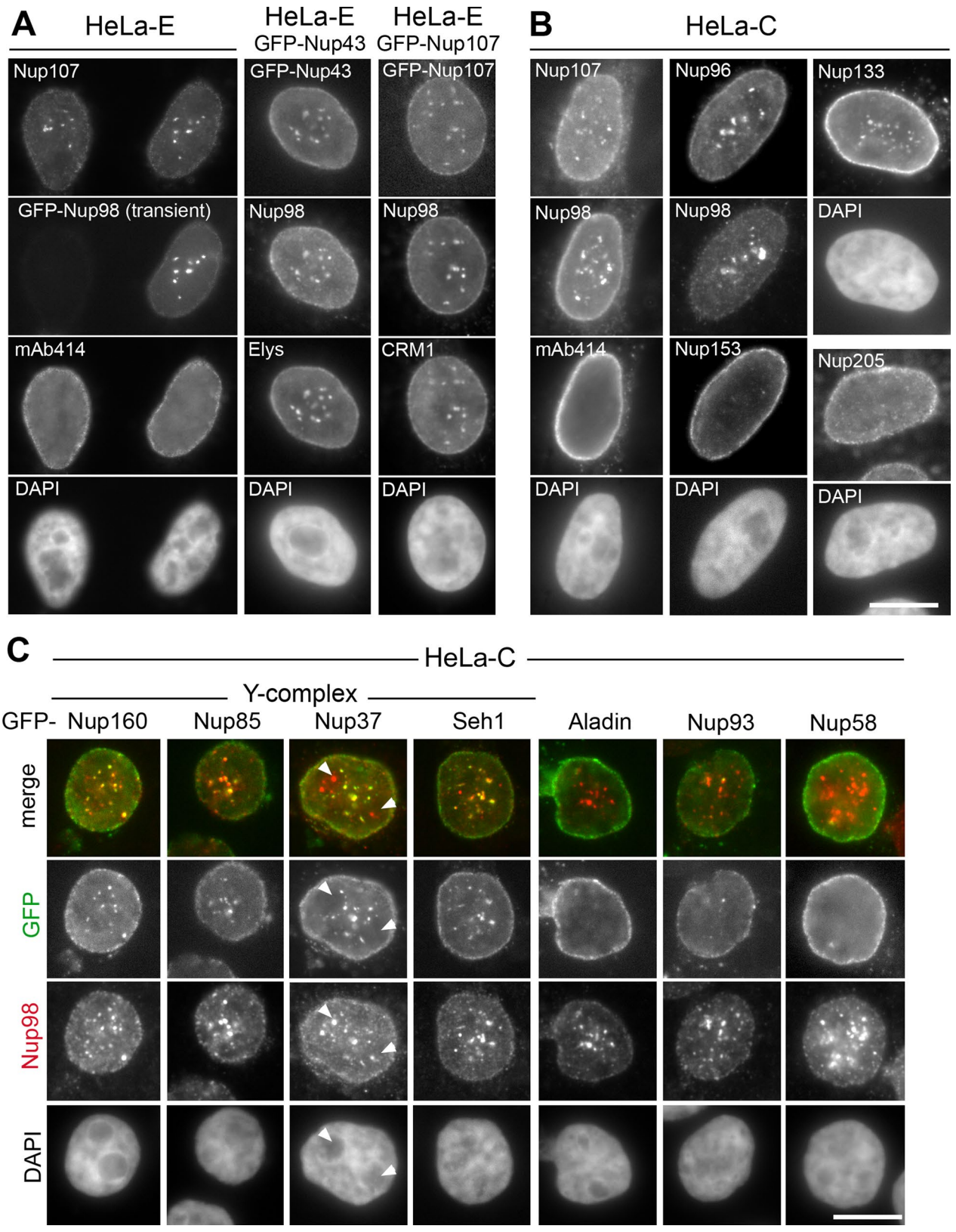


FIGURE 1: The Y-complex colocalizes with Nup98 and Elys in intranuclear bodies in HeLa cells. (A) HeLa-E cells transiently transfected with GFP-Nup98 (left) or stably expressing GFP-Nup43 (middle) or GFP-Nup107 (right) were stained with the indicated antibodies and DAPI. The GFP-Nups signals are also shown. (B) HeLa-C cells were stained with the indicated antibodies and DAPI. (C) HeLa-C cells transiently transfected with the indicated GFP fusions were fixed 3 d after transfection and stained with anti-Nup98 antibody and DAPI. Top, merge signals between the GFP (green) and the Nup98 staining (red). Arrowheads point to foci localized within the nucleolus that are stained with Nup98 but not GFP-Nup37 or Elys. Bars, 10 μm.

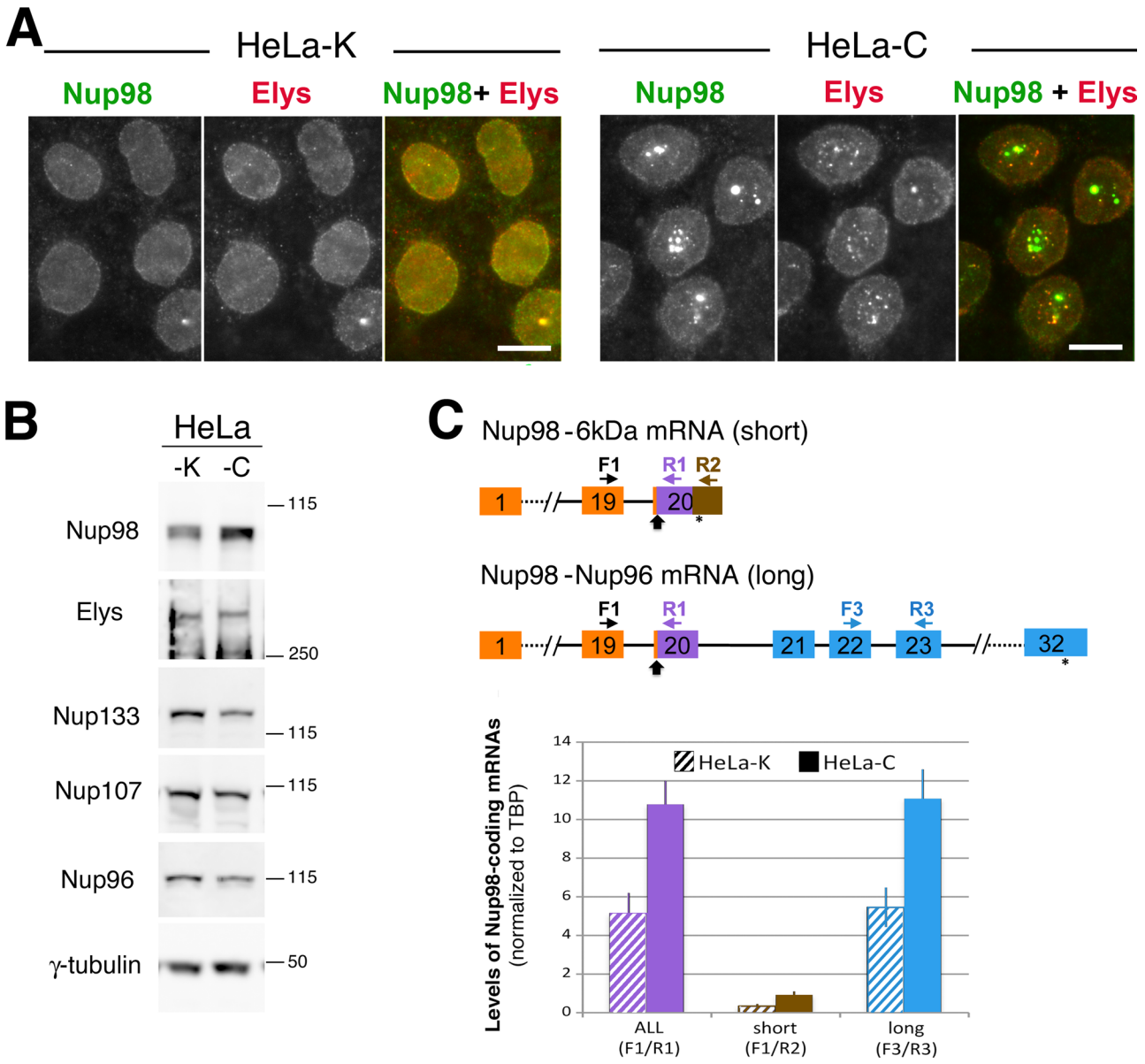


FIGURE 2: The presence of multiple GLFG bodies containing Elys and the Y-complex is linked to increased Nup98 levels in HeLa-C cells. (A) HeLa-K and HeLa-C cells were stained with anti-Nup98 and anti-Elys antibodies. Right, merged signals. Scale bars, 10 μm. (B) Western blot analysis of Nup98, Elys, and several Y-Nups in total cell extracts from HeLa-K and HeLa-C cells. γ-Tubulin is used as loading control. Molecular masses are indicated (kilodaltons). (C) Top, schematic representation of the Nup98-6kDa and Nup98-Nup96 transcripts. Nup98-encoding exons (1–19 and first nucleotides of exon 20) and Nup96-specific exons (21–32 are colored in orange and blue, respectively). Exon 20 codes for a shared sequence between the 6-kDa peptide and the beginning of Nup96 (purple); upon alternative splicing, exon 20 further encodes for six amino acids and the noncoding sequence specific for Nup98-6kDa transcript (brown). Stars indicate the position of the mRNA stop codons and the arrow the site of autoproteolytic cleavage on the resulting proteins. The position of the primers used for qRT-PCR is also indicated. Bottom, qRT-PCR analysis of Nup98-6kDa and Nup98-Nup96 mRNA levels in HeLa-K and HeLa-C cells. Values were normalized to TBP mRNA levels. Means and SD arise from three independent mRNA samples for each strain.

Unlike Y-Nups and Elys, the other nucleoporins assayed using antibodies (Nup205, Nup153, Tpr, and RanGAP1, as well as the FG-Nups recognized by mAb414) or GFP fusions (Nup58, Nup93, and Aladin) were not detected in these intranuclear bodies (Figure 1, B and C, and Table 1). Although lack of epitope accessibility cannot be formally excluded for some Nups, these data clearly indicate that not all nucleoporins are recruited to these bodies. Finally, and in agreement with the initial characterization of GLFG bodies in cells transiently overexpressing Nup98 (Griffis *et al.*, 2002), no colocalization could be detected in HeLa-E or HeLa-C cells with markers of other well-characterized intranuclear structures, including coilin, SC35, PML, Rad51, or centromeric proteins (Table 1; unpublished data).

Taken together, these results revealed that in addition to their localization at NPCs, the Y-complex and Elys are found inside the nucleus, where they can be specifically recruited, together with Nup98 and CRM1, to GLFG bodies.

| | | Ab | GFP |
|---|---|---|---|
| Y-complex + Elys | Nup160 | | + (1C) |
| | Nup133 | + (1B) | + |
| | Nup107 | + (1A, B) | + (1A) |
| | Nup96 | + (1B) | + (3D) |
| | Nup85 | | + (1C) |
| | Nup43 | | + (1A) |
| | Nup37 | | + (1C) |
| | Seh1 | | + (1C) |
| | Elys | + (1A, C) | + |
| Other Nups and transport factors | Nup205 | – (1B) | |
| | Nup93 | | – (1C) |
| | Nup58 | | – (1C) |
| | Aladin | | – (1C) |
| | mAb414 "FG-Nups" | – (1A, B) | |
| | Nup153 | – (1B) | |
| | Tpr | – | |
| | RanGAP1 | – | |
| | CRM1 | + (1A) | |
| | Gle2/Rae1 | | + (S1A) |
| Markers from other nuclear compartments | CNoBs (GFP-CPEB1)[a] | | + (S1B) |
| | Coiled bodies (coilin) | – | |
| | Specles (SC35) | – | |
| | PML bodies (PML) | – | |
| | DNA repair foci (Rad51) | – | |
| | Centromeres (CREST serum) | – | |

The last two columns indicate localizations that were analyzed using either specific antibodies (Ab) and/or transfected GFP fusions (GFP). +, colocalization with Nup98 in GLFG bodies; –, no detectable localization in intranuclear bodies. The parentheses in the last two columns indicate the figures or supplemental figures in which the corresponding localization is shown.
[a]GFP-CPEB1 is a translational regulator previously reported to colocalize upon overexpression with CRM1 into intranuclear bodies most often associated with nucleoli and thus referred to as "Crm1 nucleolar bodies" (CNoBs; Ernoult-Lange *et al.*, 2009). The colocalization of GFP-CPEB1 with Nup98 and Elys (Supplemental Figure S1B) and the fact that CNoBs were not detected in all HeLa sublines (Lin *et al.*, 2010) strongly suggest that these structures correspond to GLFG bodies.

**TABLE 1:** Nucleoporins, transport factors, and nuclear proteins analyzed for localization in Nup98-containing nuclear bodies.

### Increased level of Nup98 is key to the appearance of Elys- and Y-complex–containing GLFG bodies

Unlike in the HeLa-E and HeLa-C sublines, endogenous GLFG bodies were only rarely detected in cells from the recently sequenced HeLa subline HeLa-K (Landry *et al.*, 2013; Figure 2A). Because transient overexpression of Nup98 was previously reported to induce its accumulation within GLFG bodies, we compared Nup98 levels in HeLa-K and HeLa-C cell lines. Western blot analyses revealed approximately twofold increase of Nup98 protein levels in HeLa-C as compared with HeLa-K cells (Figure 2). In contrast, neither Elys nor any of the Y-Nups assayed showed an increased level in HeLa-C cells. We next performed quantitative reverse transcription PCR (qRT-PCR) on total RNAs extracted from these two cell lines, using primers recognizing either all Nup98-containing transcripts or only the short (Nup98-6kDa) or long (Nup98-Nup96) mRNAs. This analysis revealed that the levels all Nup98-encoding mRNAs were increased by twofold to threefold in HeLa-C as compared with HeLa-K cells (Figure 2C). This study also revealed that in both HeLa sublines, the long Nup98-Nup96 transcripts were much more abundant than the short ones solely encoding Nup98 (as also originally described by Fontoura *et al.*, 1999). Taken together, these results indicate that in HeLa-C cells, the increased protein level of Nup98 is linked to increased transcription or stability of the Nup98-Nup96 mRNAs and not to major changes in alternative splicing favoring the expression of the short Nup98-6kDa mRNAs.

The increased levels of Nup98 in HeLa-C cells prompted us to determine the consequences of Nup98 overexpression in cells largely devoid of GLFG bodies. As shown in Figure 3B, immunofluorescence analysis of HeLa-K cells stably expressing mCherry-Nup107 revealed the recruitment of Elys and mCherry-Nup107 into most of the GLFG bodies induced by GFP-Nup98 overexpression. Similar recruitment of Elys into these GLFG bodies was also observed in HeLa-K cells (Supplemental Figure S2). Together these data thus revealed that increased Nup98 levels are sufficient to recruit Elys and Y-Nups into the induced GLFG bodies.

### The C-terminal domain of Nup98 contributes to the recruitment of Elys and the Y-complex to nuclear bodies

We next sought to determine how Nup98 recruits the Y-complex and Elys to the GLFG bodies. We therefore overexpressed in HeLa-K cells a GFP-Nup98 N-terminal construct (GFP-Nup98$^{1\text{-}469}$) that carries most of the cohesive GLFG/FG repeat domain of Nup98. This truncated form lacks the C-terminal domain of Nup98 and is not targeted to the NPCs but accumulates within GLFG bodies (Griffis *et al.*, 2002; Xu and Powers, 2010). Unlike full-length Nup98, overexpression of GFP-Nup98$^{1\text{-}469}$ in HeLa-K cells did not lead to recruitment of Elys or mCherry-Nup107 into the newly formed nuclear bodies (Figure 3B and Supplemental Figure S2). These data thus indicate a critical role for the C-terminal domain of Nup98 in the recruitment of Elys and the Y-complex into GFLG bodies. Of note, HeLa-C cells overexpressing GFP-Nup98$^{1\text{-}469}$ most often displayed fewer Elys-positive GLFG bodies than did nontransfected cells (Supplemental Figure S2). Thus this truncated form of Nup98 appears to exert a dominant-negative effect on preexisting GLFG bodies in HeLa-C cells (see *Discussion*).

The C-terminal domain of Nup98, which is absent from GFP-Nup98$^{1\text{-}469}$, includes the region required for interaction with the N-terminus of Nup96 (Griffis *et al.*, 2003). To determine whether this interaction contributes to the recruitment of Nup96 to the GLFG bodies, we transfected HeLa-C cells with an N-terminal epitope–tagged form of Nup96 (GFP-Nup96) that was reported to abolish its binding to Nup98 (Griffis *et al.*, 2003). As a control, cells were transfected with a C-terminally tagged form of Nup96 (Nup96-GFP). As shown in Figure 3C, both GFP-Nup96 and Nup96-GFP were properly targeted to the NPCs, indicating that these fusions can be assembled within Y-complexes. However, unlike Nup96-GFP, the GFP-Nup96 fusion was not targeted to the existing GLFG bodies in

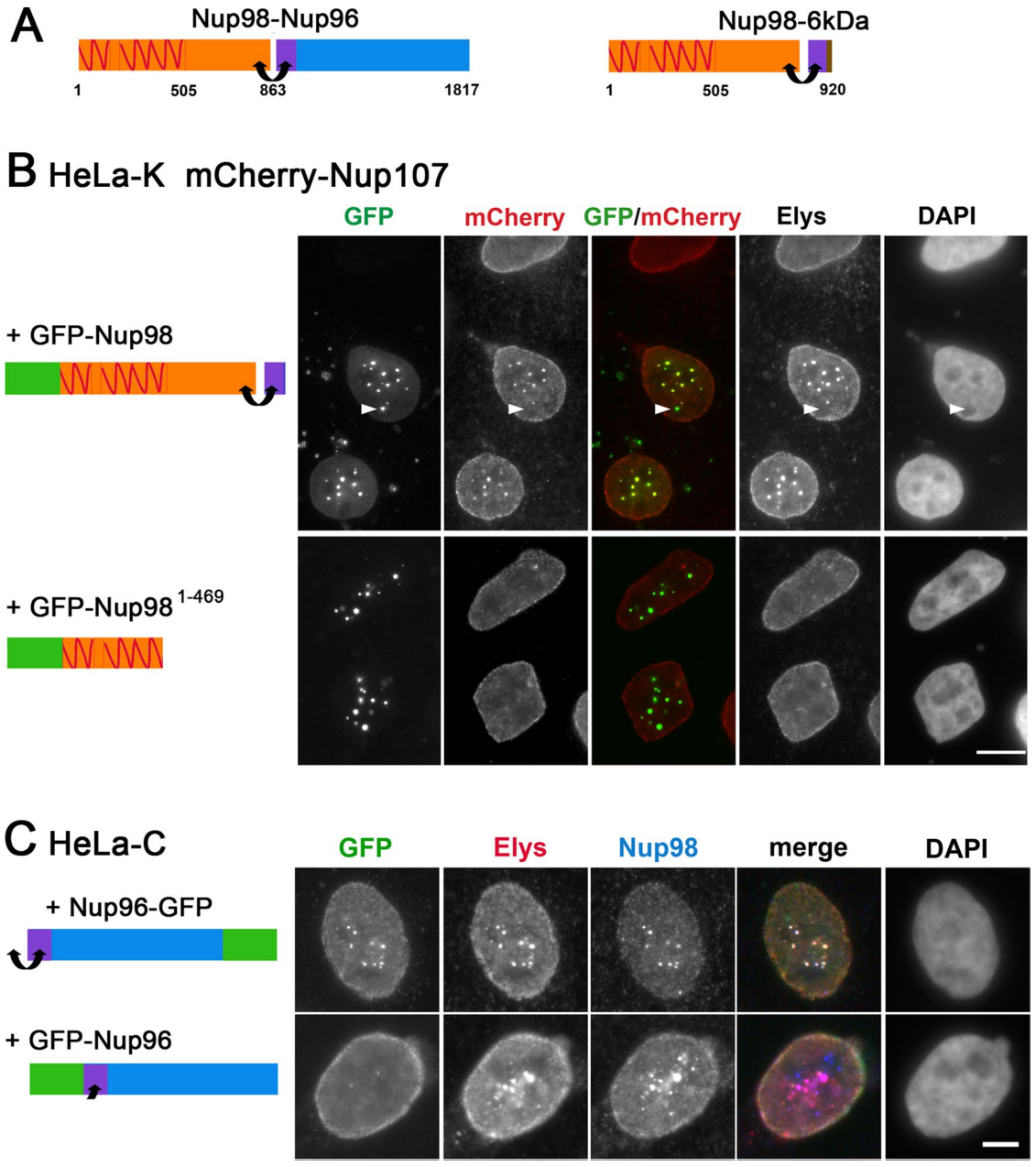


FIGURE 3: The C-terminal domain of Nup98 contributes to the recruitment of Elys and the Y-complex to intranuclear bodies. (A) Schematic representation of the Nup98-Nup96 and Nup98-6kDa protein precursors. GLFG repeat domains within the N-terminal of Nup98 (red zigzags) and the interactions (double arrow) between the C-terminal domain of Nup98 and either the N-terminal domain of Nup96 or the 6-kDa peptide (purple) are indicated. (B) HeLa-K cells stably expressing mCherry-Nup107 were transfected with plasmids expressing full-length GFP-Nup98 or a C-terminal-truncated GFP-Nup98 construct (GFP-Nup98$^{1-469}$). Cells were fixed 18 h after transfection and stained with anti-Elys and DAPI. Localization of the transfected GFP-Nup98 fusions (GFP), the stably expressed mCherry-Nup107 (mCherry), and Elys is presented along with the merge of the GFP and mCherry signals. The arrowhead points to a body localized within the nucleolus that, unlike nucleoplasmic GLFG bodies, contains GFP-Nup98 but not mCherry-Nup107 or Elys. Scale bar, 10 μm. (C) HeLa-C cells were fixed 3 d after transfection with Nup96-GFP (binds Nup98) or GFP-Nup96 constructs (cannot bind Nup98) and immunostained with anti-Elys and anti-Nup98 antibodies. The merge of all three stainings is also shown. Bar, 5 μm.

HeLa-C cells (Figure 3C). (Note that the presence of endogenous Nup96 likely accounts for the persistence of Elys in GLFG bodies in GFP-Nup96–expressing HeLa-C cells.) Together these data indicate that the Nup98-C terminal domain contributes to the recruitment or maintenance of the Y-complex and Elys in intranuclear GLFG bodies, most likely through its interaction with Nup96.

### Behavior of Elys and Y-Nups compared with Nup98 in intranuclear bodies

We next investigated the localization of the Y-complex and Elys upon treatment with drugs previously reported to affect GLFG bodies. Leptomycin B (LMB), a specific inhibitor of the nuclear export receptor Crm1, was previously reported to interfere with the

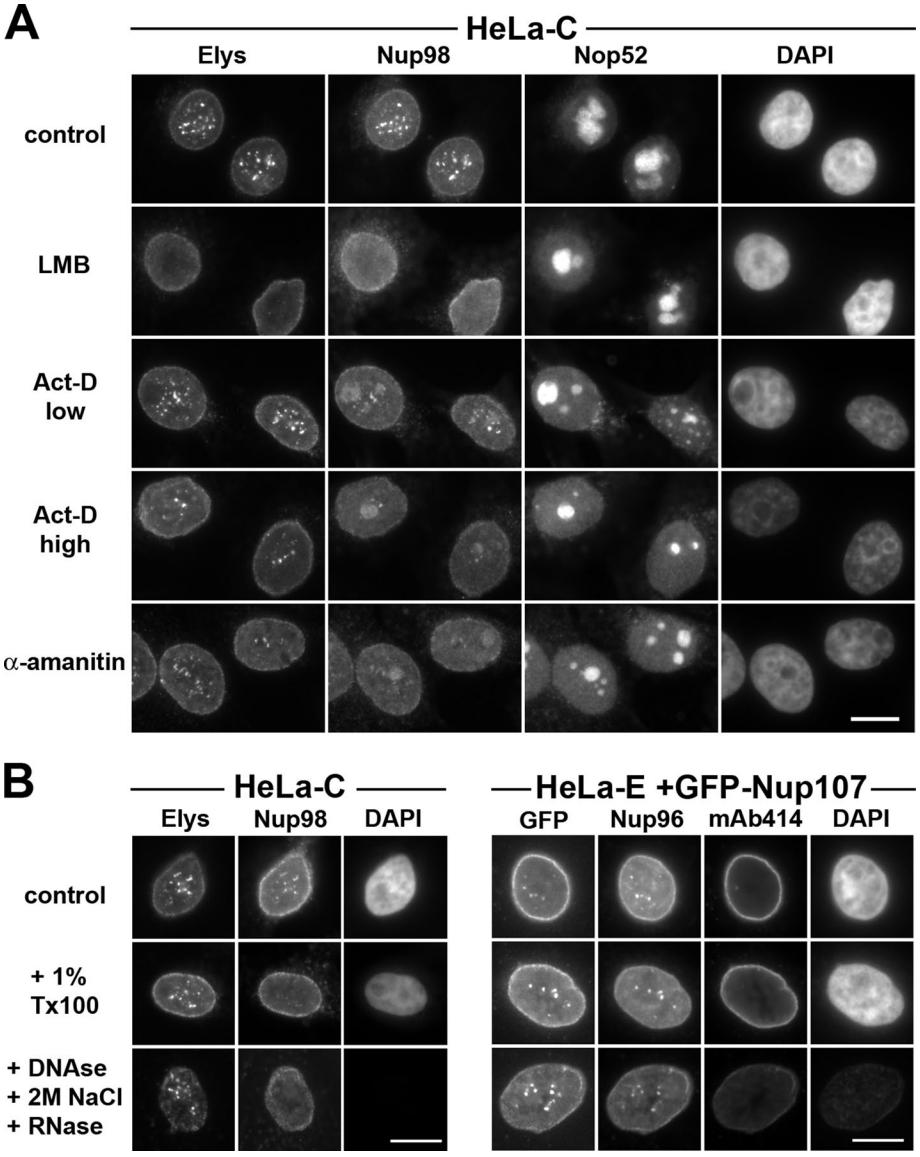


FIGURE 4: Compared behavior of Elys, Nup98, and Y-Nups upon LMB, Act-D, or α-amanitin treatment or after sequential cellular extractions. (A) HeLa-C cells were treated for 2 h with 20 nM LMB or actinomycin-D at 50 ng/ml (low) or 5 µg/ml (high) or for 4 h with 50 µg/ml α-amanitin. Cells were then fixed and immunostained with anti-Elys, anti-Nup98, and anti-Nop52. DAPI staining was used to visualize nuclei. (B) HeLa-C cells (left) or HeLa-E cells stably expressing GFP-Nup107 (right) were submitted to in situ extraction with 1% Triton X-100 (+1% Tx100), followed by sequential DNase I, 2 M NaCl, and RNase A extractions before fixation. Cells were then immunostained with the indicated antibodies. The efficiency of chromatin digestion is attested by the disappearance of the DAPI staining. Bars, 5 µm.

localization of overexpressed GFP-Nup98 within GLFG bodies (Oka *et al.*, 2010). Upon treatment of HeLa-C cells with LMB, endogenous Nup98 and Elys were no longer detected within intranuclear bodies (Figure 4A). Similarly, GFP-Nup107 and GFP-Nup43, stably expressed in HeLa-E cells, were no longer localized within nuclear bodies upon LMB treatment (unpublished data). This indicates that Crm1 plays a key function in the assembly or maintenance of these nuclear bodies.

In contrast, other cell treatments differentially affected the nuclear localization of Nup98 as compared with Elys or Y-Nups. Indeed, consistent with a previous study (Oka *et al.*, 2010), we observed that transcriptional inhibitors such as actinomycin D (Act-D) or α-amanitin led to the nucleolar accumulation of Nup98 and its progressive disappearance from the intranuclear bodies. In contrast, Elys did not accumulate in nucleoli, and its localization within nuclear foci was less affected by these treatments (Figure 4A). In addition, the fraction of Nup98 present in intranuclear bodies was readily solubilized by 1% Triton extraction, whereas Elys, Nup96, GFP-Nup107, and GFP-Nup43 staining in nuclear bodies was resistant to sequential extraction with 1% Triton, DNase I, 2 M NaCl, and RNase A (Buckler-White *et al.*, 1980; Figure 4B; unpublished data). This indicates that once recruited to intranuclear foci, Elys and Y-complex constituents become associated with a stable nuclear structure, whereas the bulk of Nup98 might be more dynamically associated.

### Dynamics of Y-Nups–, Elys-, and Nup98-containing nuclear bodies during the cell cycle

To characterize further these Y-complex–containing intranuclear bodies, we monitored their dynamics throughout the cell cycle. Time-lapse sequences of live HeLa-E cells stably expressing GFP-Nup107 (Figure 5A) or GFP-Nup43 (unpublished data) revealed a progressive disassembly of the intranuclear bodies that was completed in most cells ~30 min before NPC and nuclear envelope disassembly (Figure 5, A and B). Similarly, immunofluorescence studies in HeLa-C cells revealed that Elys and Nup98 signals within foci decreased both in number and intensity in late G2 cells, as characterized by a discontinuous phospho-H3 staining (Hendzel *et al.*, 1997). GLFG bodies were no longer detectable in prophase cells (defined by a strong and continuous phospho-H3 staining but persistent staining of Elys at the nuclear rim; Figure 5C). After mitosis, reassembly of these bodies was progressive in HeLa-E cells (Figure 5, A and B) but likely occurs faster in HeLa-C cells, as revealed by the presence of multiple intranuclear bodies in most cells (Figure 5C).

GLFG bodies, including the Y-complex Nups and Elys, are therefore disassembled and reformed during cell cycle progression. Of importance, this dynamic behavior highlights the fact that these structures are not simply a result of aggregation, but instead that specific regulations can modulate these protein assemblies in a cell cycle–dependent manner.

### Y-Nups shuttle between nuclear bodies and the nucleoplasm

We next characterized the intranuclear dynamics of Y-Nups in interphase, taking advantage of our HeLa-E cell lines stably expressing GFP-Nup107 or GFP-Nup43. Consistent with previous studies (Rabut *et al.*, 2004), photobleaching of the nuclear envelope did not lead to any detectable recovery of the GFP-Y-Nups signals over

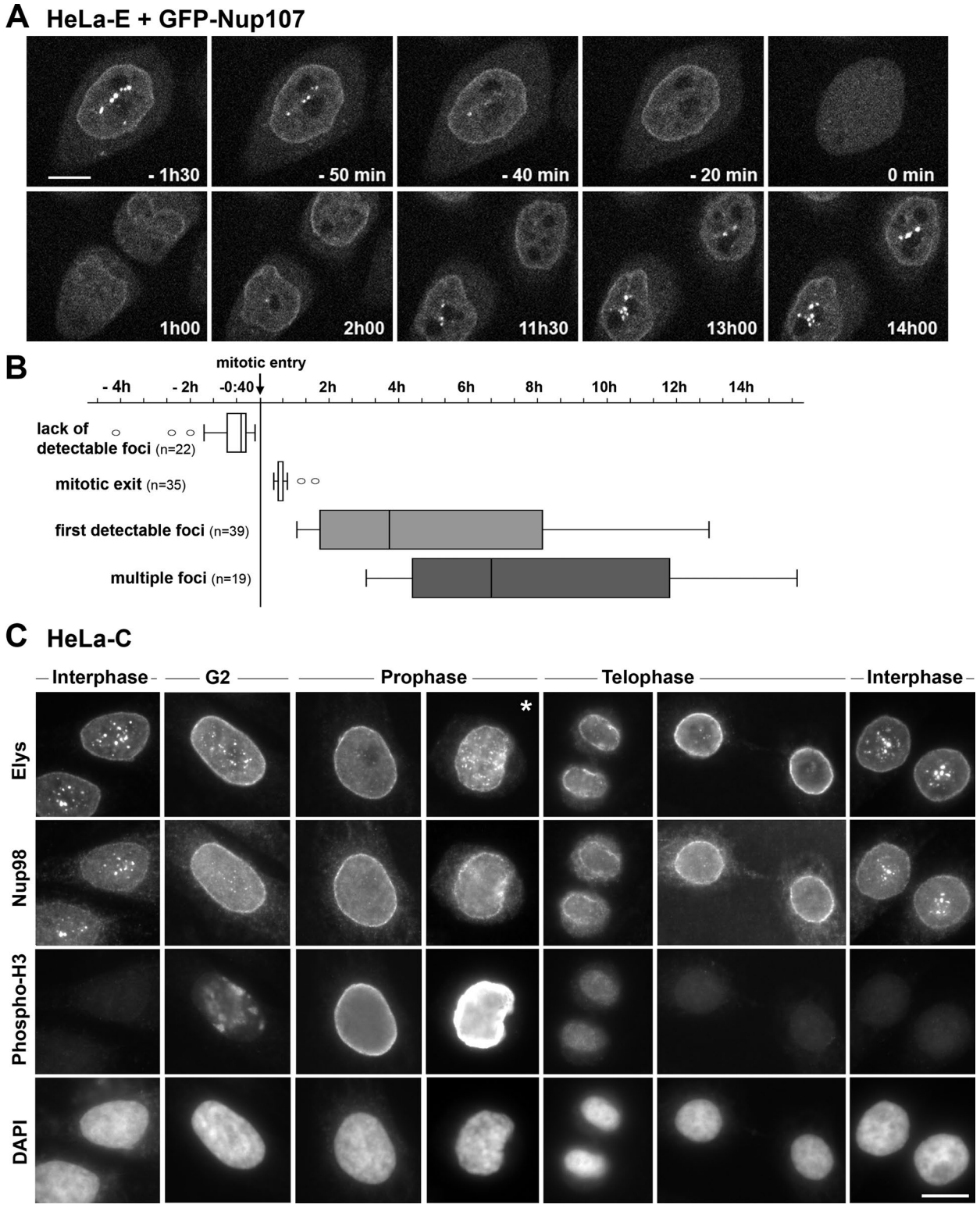


FIGURE 5: Cell cycle dynamics of GFP-Nup107–, Elys-, and Nup98-containing nuclear bodies. (A) Representative time frames of a HeLa-E cell stably expressing GFP-Nup107 analyzed by spinning-disk confocal microscopy at various stages of the cell cycle. One single *Z*-plane is shown. Time 0 was set at mitotic entry. Scale bar, 10 μm. See also Figure 5_movie .mov. (B) Quantification of the kinetics of foci disassembly and reassembly in HeLa-E cells stably expressing GFP-Nup107. The number of cells imaged is indicated. Mitotic entry was defined as the first time frame at which cell rounding was observed and mitotic exit as the first frame where two distinct nuclei were detectable. The disappearance and reappearance of foci was manually recorded on individual dividing cells. Box plots were generated using KaleidaGraph (see *Materials and Methods*). (C) HeLa-C cells triple stained with anti-Elys, anti-Nup98, and anti–phospho-histone H3 and DAPI. Typical stages of the cell cycle are shown. The star denotes a late-prophase cell in which kinetochores staining by Elys becomes detectable. Scale bar, 10 μm.

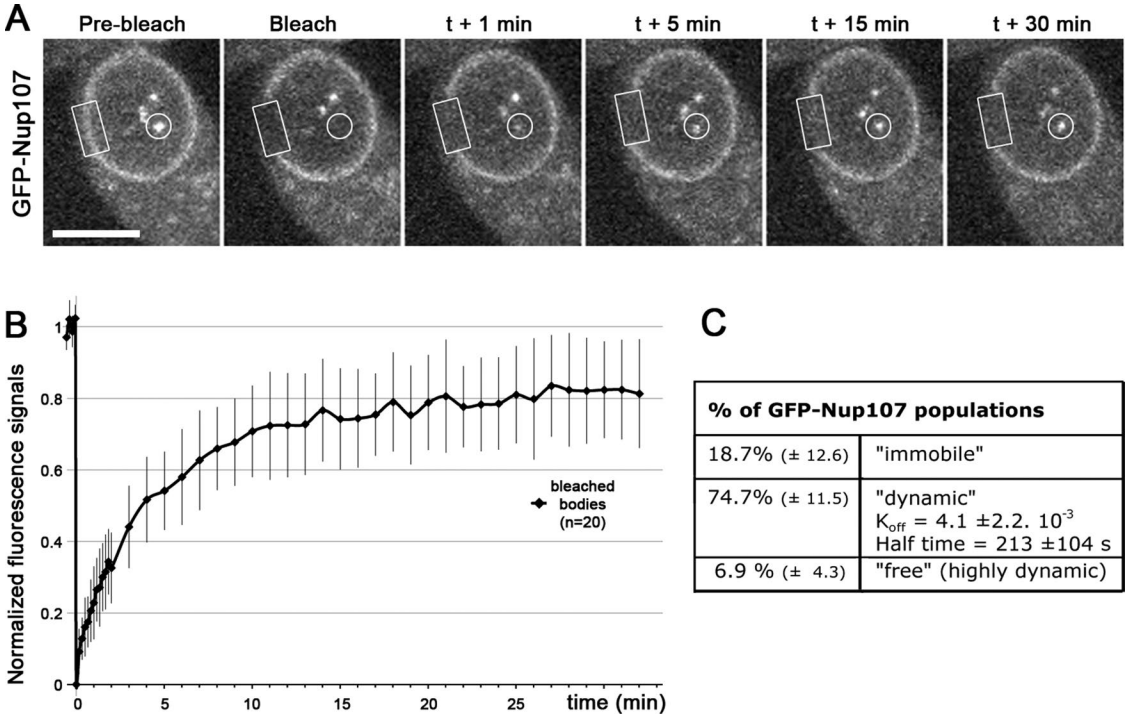


FIGURE 6: Quantitative FRAP analysis of GFP-Nup107 dynamics in nuclear bodies. (A) Time frames of a representative FRAP series of a HeLa-E cell stably expressing GFP-Nup107 recorded with spinning-disk confocal microscopy. The bleached nuclear body (circle) and NE area (rectangle) are indicated. Time 0 was defined as the first time point after bleach. Scale bar, 10 µm. See also Figure 6_movie.mov. (B) The average normalized fluorescence signals of 20 bleached bodies and corresponding SDs plotted vs. time. (C) Fractions of the various GFP-Nup107 populations exhibiting distinct dynamics within the nuclear bodies were determined based on the fit of the normalized fluorescence signals using a reaction-dominant model. See also *Materials and Methods*, Supplemental Figure S3, and Figure S3_movie.mov.

30 min. In contrast, GFP-Nup107 and GFP-Nup43 recovery was clearly detectable when nuclear bodies were bleached (Figure 6A and Supplemental Figures S3A and S4). After quantifications (Figure 6B and Supplemental Figure S3, B and C), the GFP-Nup107 recovery curves of the bleached bodies were fitted using a reaction-dominant model involving a unique binding state (Supplemental Figure S3D; see *Materials and Methods*). This analysis revealed that most of the GFP-Nup107 fluorescence in the nuclear bodies recovers with a half-time of ~3–4 min (Figure 6C). Thus, in contrast to their behavior at the NPCs, Y-Nups are dynamic within the GLFG bodies. These findings further highlight the existence of a nucleoplasmic pool of Y-Nups able to exchange dynamically with the fraction present in the nuclear bodies.

To better characterize this nucleoplasmic pool, we next photobleached half of the nucleus and watched the subsequent recovery of fluorescence (Figure 7 and Supplemental Figure S5). Under those conditions, the signal within the nuclear bodies recovered with kinetics comparable to the ones observed when only the intranuclear bodies were bleached. Although the overall recovery within the rest of the nucleoplasm appeared faster, with ~35% of the signal recovering within the first 10 s, subsequent intranuclear recovery was far slower, reaching ~80% within only 5–10 min, and was not complete after 30 min. This indicates that within the nucleoplasm, Nup107 exists in multiple fractions: a very mobile one, and fractions with far more restricted diffusion.

## DISCUSSION

Previous studies pointed to the existence of intranuclear fractions of several Y-complex subunits and Elys in human cells (Enninga *et al.*, 2003; Rasala *et al.*, 2006; Bilokapic and Schwartz, 2013; Schwartz *et al.*, 2015). Here the use of specific HeLa cell lines displaying high frequency of GLFG bodies provides the first evidence of the colocalization of all Y-complex subunits analyzed and Elys, along with Nup98 and CRM1, within a subset of GLFG bodies (Figure 1). The presence of Y-Nups and Elys in GLFG bodies seems quite specific, as none of the other Nups analyzed using antibodies or GFP fusions were detectable within these bodies (Table 1).

We further demonstrate that the increased occurrence of GLFG bodies in HeLa-C compared with HeLa-K cells is correlated with increased Nup98 protein levels. However, despite approximately twofold increase in mRNA level observed for the Nup98-Nup96 precursor (which represents the major Nup98-encoding transcript in all HeLa cell lines we analyzed), Nup96 proteins levels were not higher in HeLa-C cells than in HeLa-K cells (Figure 2). Although other cellular mechanisms cannot be excluded, this discrepancy between Nup98 and Nup96 mRNAs versus protein levels may be linked to posttranslational regulations of Nup96 that lead to its proteasome-mediated degradation during mitosis (Chakraborty *et al.*, 2008).

Consistent with the increased levels of Nup98 in HeLa-C cells, we further showed that transient overexpression of Nup98 in HeLa-K cells is sufficient to induce the recruitment of the Y-complex and Elys to most of the induced GLFG bodies (Figure 3B and Supplemental Figure S2). Conversely, conditions known to induce the disassembly of GLFG bodies, such as LMB (Oka *et al.*, 2010), or overexpression of a GFP-Nup98-HoxA9 fusion led to the disappearance of Elys and the Y-complex subunits from intranuclear bodies in HeLa-C cells (Figure 4A, Supplemental Figure S2, and unpublished data). Our data further indicate that the C-terminal domain of

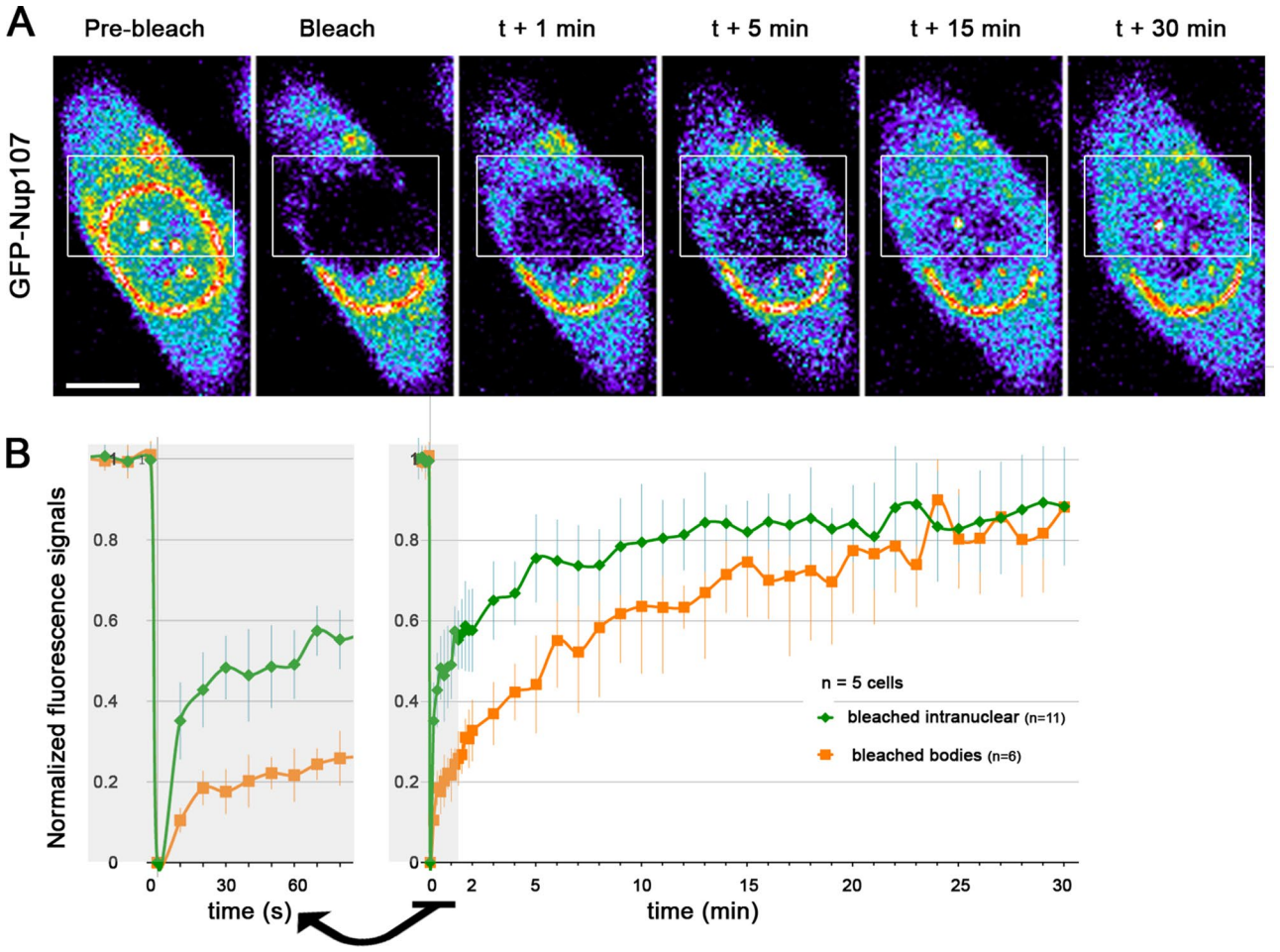


FIGURE 7: Quantitative FRAP analysis of GFP-Nup107 intranuclear dynamics. (A) Pseudocolor images of time frames of a representative FRAP series of a HeLa-E cell stably expressing GFP-Nup107 recorded with spinning-disk confocal microscopy. The bleached area (rectangle) that encompasses approximately half of the nucleus and a fraction of the cytoplasm is indicated. Time 0 was defined as the first time point after bleach. Scale bar, 10 µm. See also Figure 7_movie .mov. (B) Average normalized fluorescence signals quantified from five bleached cells (6 nuclear bodies and 11 intranuclear areas) and corresponding SDs plotted vs. time. The gray-shaded area is shown at two time scales to better visualize the first time points of the curves. Note that since ~45–65% of the intranuclear signal was initially bleached, depending on cells, the double normalization (required to allow comparison among cells) accounts for the apparent discrepancy between the partial recovery visualized on the images in A (*t* + 30 min compared with prebleach) and the normalized fluorescence signals values in B, which should reach 100% in the absence of any "immobile" fraction. See also *Materials and Methods* and Supplemental Figure S5.

Nup98 clearly contributes to the recruitment or stability of the Y-complex and Elys to the GLFG bodies, a process that likely involves the interaction between Nup98 and Nup96 (Griffis *et al.*, 2003; Figure 3, B and C, and Supplemental Figure S2). However, other determinants, possibly including Y-complex–independent interactions between Elys and Nup98 (Schwartz *et al.*, 2015), also appear to contribute to this process. Of interest, Elys encompasses within its C-terminal disordered region a putative AT-hook DNA-binding motif and an additional domain required for chromatin binding. In addition, it physically associates on chromatin with the Mcm2-7 replication-licensing proteins (Gillespie *et al.*, 2007; Rasala *et al.*, 2008). These properties of Elys and/or additional partners of the Y-complex or Elys may explain their persistence within nuclear bodies upon extraction conditions defined as "nuclear matrix" preparation that lead to the removal of most if not all Nup98 (Figure 4B).

Of note, Elys was also largely displaced from these bodies upon overexpression in HeLa-C cells of a GFP-Nup98$^{1\text{-}469}$ construct derived from the GFP-Nup98-HoxA9 fusion but lacking the HoxA9 domain. This result was somewhat unexpected, as this fusion still forms intranuclear bodies that should recruit endogenous Nup98. However, earlier FRAP experiments indicated that GFP-Nup98$^{1\text{-}469}$ recovered less quickly and thus was more tightly associated in GLFG bodies than was the full-length protein (Xu and Powers, 2010). Thus it is possible that Nup98$^{1\text{-}469}$ displaces the full-length protein, with the consequence that Y-complex interaction sites are reduced. Alternatively, this observation may reflect the existence of distinct subsets of GFLG bodies. Indeed, unlike CRM1 and Rae1/Gle2-GFP, Elys and Y-Nups were not detectable in a subset of Nup98-containing nuclear foci, most frequently those localized within the nucleolus (arrowheads in Figure 1C and Supplemental Figures S1 and S2). This may be caused by a lack of accessibility of the Nup98-binding site and/or an impaired accessibility of the Y-complex and Elys to specific nuclear domains. In line with this hypothesis, it was recently demonstrated that Nup98, when targeted to tandem copies of a LacO-containing DNA array in U2OS cells, does not recruit Y-Nups to this LacO array (Schwartz *et al.*, 2015).

Our study of Y-complex dynamics revealed the progressive disassembly of these nuclear bodies that initiates ~1 h before mitotic entry, coincidently with histone H3 phosphorylation, and is completed ~20–30 min before NE breakdown (Figure 5). GLFG body disassembly thus seems to precede the weakening of the NE barrier that was previously correlated with a specific phosphorylation of Nup98 by multiple kinases (Laurell *et al.*, 2011). However, that study also revealed that expression of a nonphosphorylable form of Nup98 delays nuclear body disassembly and that a Nup98 phosphomimetic mutant is targeted with lower efficiency to intranuclear bodies (Laurell *et al.*, 2011; Laurell and Kutay, 2011). It is thus possible that cell cycle–dependent phosphorylations on Nup98 affect both nuclear bodies and NPCs, albeit with different kinetics. In the future, it will be interesting to determine the extent to which changes in GLFG cohesiveness, Nup98-Nup96 interactions, and/or chromatin binding properties of Elys contribute to the dynamics of these nuclear bodies throughout the cell cycle.

Analysis of the mobility of GFP-Nup107 and GFP-Nup43 during interphase indicated that most of the fluorescence in the nuclear bodies recovers with a similar half-time of ~3 min (Figure 6 and Supplemental Figure S4), suggesting that the Y-complex is likely recruited as complete entity, possibly along with Elys, to these bodies. In contrast, this exchange rate appears to be far slower that the previously reported dynamics of Nup98, whose half-time of fluorescence recovery was found to be of ~12 s with an immobile GFP-Nup98 fraction of ~25% (Griffis *et al.*, 2002). Because in that study GFP-Nup98 recovery was followed over only 2–3 min, the "immobile" fraction may correspond to a slowly exchanging pool of Nup98 to which the Y-complex and Elys would bind. The existence of distinct pools of Nup98 within the GLFG bodies could possibly explain the apparent earlier dissociation from the nuclear bodies of a pool of Nup98 as compared with Elys upon transcription inhibition or in late G2 (Figures 4A and 5C).

Beyond the detection within nuclear bodies, our FRAP experiments clearly established the presence of an intranuclear pool of Nup107 or Nup43 able to exchange dynamically with these bodies (Figures 6 and 7 and Supplemental Figure S4). Experiments performed on half-bleached nuclei further indicate that although a large fraction of GFP-Nup107 is highly dynamic, leading to a significant recovery within the first 10–20 s, the rest of the intranuclear pool recovers with a slower rate, similar to the one observed within the nuclear bodies. This less mobile fraction likely reflects the dynamic association of Nup107 embedded within Y-complexes, possibly along with Elys and Nup98, with dispersed intranuclear binding sites.

Because endogenous GLFG bodies have so far been detected only in the *Xenopus* A6 and XL177 cell lines and in several HeLa sublines, their physiological relevance remains elusive. However, our study demonstrates the existence of an intranuclear pool of the Y-complex, even in HeLa-K cells largely devoid of GLFG bodies, which likely underscores a more general function of this complex. At this stage, we can only speculate about the function of the intranuclear pool of the Y-complex during interphase. Although this fraction may possibly underlie the requirement of nuclear Y-complex for interphase NPC assembly (D'Angelo *et al.*, 2006), we do not favor this hypothesis, since Elys is dispensable for NPC assembly at this stage of the cell cycle (Doucet *et al.*, 2010). On the other hand, our data revealed that the Y-complex and Elys can interact with Nup98, at least within GLFG bodies. These nucleoporins may thus contribute to some of the previously described intranuclear functions of Nup98 during interphase. The fact that unlike Nup98, Y-Nups and Elys do not relocalize inside the nucleolus upon transcription inhibition indicates that these Nups do not contribute to all Nup98 functions in RNA processing and trafficking (Oka *et al.*, 2010). Similarly, whereas a role for a non–NPC-bound fraction of Nup98 in transcriptional memory was established, the authors reported that Nup107 depletion does not affect this process (Light *et al.*, 2013). In the future, it will be interesting to determine whether the intranuclear fraction of the Y-complex contributes to other known functions of Nup98 in transcriptional or posttranscriptional gene regulation (Singer *et al.*, 2012; Liang *et al.*, 2013) or in other nuclear processes. Earlier work revealing the kinetochore localization of the Y-complex and Elys was critical in pioneering the roles of nucleoporins in mitosis (reviewed in Wozniak *et al.*, 2010). Similarly, we anticipate that this study will pave the way for further exciting discoveries on novel functions of the Y-complex during interphase.

## MATERIALS AND METHODS

### Cell culture and plasmid transfections

HeLa cells were grown at 37°C in DMEM (Invitrogen, Carlsbad, CA) supplemented with 10% fetal calf serum, 1% L-glutamine, 100 µg/ml streptomycin, and 100 U/ml penicillin. HeLa-E is a subclone of HeLa cells initially received from F. Perez (Institut Curie, Paris, France) that was used in our initial studies (Belgareh *et al.*, 2001). The HeLa-K cells were a gift from J. Ellenberg (EMBL, Heidelberg, Germany) and correspond to the recently sequenced HeLa subline (Landry *et al.*, 2013). The HeLa-C subline, which features multiple endogenous GLFG bodies (Xu and Powers, 2010), was a kind gift from V. Cordes (MPIBPC, Göttingen, Germany).

Plasmids used in this study were either previously published or generated using standard molecular cloning techniques and are listed in Supplemental Table S1. Plasmid transfections were performed using Lipofectamine 2000 (Invitrogen). To establish stable cell lines (HeLa-E stably expressing GFP-Nup107 or GFP-Nup43 and HeLa-K stably expressing mCherry-Nup107), individual clones were isolated by G418 (1 mg/ml) selection.

### Immunofluorescence analyses

The following primary antibodies were used for immunofluorescence in this study: anti-Nup98 rat monoclonal (2H10; ab50610; 1/2000; Abcam, Cambridge, MA); affinity-purified rabbit antibodies directed against human Nup107 and Nup133 (Belgareh *et al.*, 2001; each at 1/400), Nup96/p87 (Fontoura *et al.*, 1999; Loiodice *et al.*, 2004; serum provided by B. Fontoura, UT Southwestern, Dallas, TX; 1/1500), and Nup205 and Nup53 (Mansfeld *et al.*, 2006; provided by U. Kutay, ETH, Zürich, Switzerland; 1/10,000 each); rabbit polyclonal anti-Elys/Mel28 antibody (FID1 serum, directed against histidine-tagged human Mel28 protein, aa 1208–1800; generously provided by R. Walczak and I. Mattaj, EMBL, Heidelberg, Germany; 1/1000); rabbit polyclonal immunoglobulin G anti-CRM1 (sc-5595, 1/100; Santa Cruz Biotechnology, Santa Cruz, CA); mouse monoclonal antibody mAb414, recognizing several FG-Nups other than Nup98 (BAbCO, Richmond, CA; 1/5000), anti-Nup153 (SA1; Bodoor *et al.*, 1999, provided by B. Burke, IMB, Singapore; 1/5), and anti–phospho-histone H3 Ser-10 (ab14955; 1/2000; Abcam); human serum C13, recognizing Nop52 (Savino *et al.*, 1999; provided by D. Hernandez-Verdun, IJM, Paris, France; 1/500). Secondary antibodies were purchased from Jackson ImmunoResearch Laboratories (West Grove, PA) or Molecular Probes (Eugene, OR).

Fluorescence signals within the intranuclear bodies were best detected upon preextraction of cells, followed by a fixation-extraction procedure. Briefly, cells were quickly preextracted for 15 s in PHEM buffer (20 mM K–1,4-piperazinediethanesulfonic acid, 10 mM K–ethylene glycol tetraacetic acid, 1 mM $MgCl_2$, pH 6.8) containing 0.2% Triton and then fixed for 10 min in the same buffer further

containing 4% paraformaldehyde supplemented with 0.85% of 1 N NaOH to the buffer to improve the detection of some antigens (Loiodice *et al.*, 2004).

To analyze the behavior of proteins within foci, monolayers of HeLa cells were submitted to in situ sequential extraction with 1% Triton X-100, 50 U/ml DNase I, 2 M NaCl, and 50 µg/ml RNase A before fixation as described (Ernoult-Lange *et al.*, 2009; a procedure referred to as "nuclear matrix" preparation). The efficiency of chromatin digestion was attested by the disappearance of the 4′,6-diamidino-2-phenylindole (DAPI) staining.

Wide-field fluorescence images were acquired using a microscope (DM6000B; Leica, Wetzlar, Germany) with a 100×, numerical aperture 1.4 (HCX Plan-Apo) oil immersion objective and a charge-coupled device (CCD) camera (CoolSNAP HQ; Photometrics, Tucson, AZ). Rapid and precise *Z*-positioning was accomplished by a piezoelectric motor mounted underneath the objective lens. Image stacks were acquired without camera binning, with a plane spacing of 0.2 µm. A single unique plane is shown in all images.

### Western blot analysis

For Western blot analysis, whole-cell lysates solubilized in SDS–PAGE sample buffer were separated on 10% or 4–12% SDS–PAGE gels and transferred to nitrocellulose filters. The resulting blots were saturated with Tris-buffered saline, 0.1% Tween, and 5% dried milk and probed with the following antibodies: anti-Nup98 rat monoclonal (2H10; ab50610; 1/2000; Abcam), polyclonal rabbit anti-Elys (A300-166A; 1/2000; Bethyl Laboratories, Montgomery, TX), rabbit polyclonal anti-hNup133 (serum #759; 1:2500; Belgareh *et al.*, 2001), anti-hNup107-Cterm (serum #520; 1:2500; Belgareh *et al.*, 2001), rabbit polyclonal anti-Nup96 (A301-784A, 1/2000; Bethyl Laboratories), and monoclonal mouse anti–γ-tubulin (ab11316, 1:10,000; Abcam). After incubation with horseradish peroxidase–conjugated secondary antibodies (Jackson ImmunoResearch Laboratories, West Grove, PA), signals were detected by enhanced chemiluminescence (SuperSignal Pico or Femto; Thermo Scientific, Lafayette, CO).

### qRT-PCR

Total RNAs were isolated using the NucleoSpin RNAII kit (Macherey-Nagel, Düren, Germany). mRNAs were reverse transcribed using random hexamers and the AMV reverse transcriptase (Finnzymes, Espoo, Finland). Real-time PCR was performed with a LightCycler 480 system (Roche, Basel, Switzerland) by using SYBR Green incorporation (SYBR Green PCR-Master Mix; Applied Biosystems, Foster City, CA), and the Nup98-containing cDNAs were amplified using the following primers (see also Figure 2): F1 AATACCGGCCTGAAACTGGT); R1 (AGGCAAAGGAGCAGTCTTCA); R2 (TCACGGATTCCATTCAAATTC); F3 (CATCCCACTCGTCGAAAACT); and R3 (AAAGATGCTGCTCTGGGAGT). The relative amounts of cDNAs in the samples were quantified according to the manufacturer's instructions and normalized by reference to the TATA-binding protein (TBP) cDNAs (using the primer pair AGTGAAGAACAGTCCAGACTG and CCAGGAAATAACTCTGGCTCAT).

### Videomicroscopy and FRAP

For spinning-disk confocal imaging, cells plated on 35-mm glass base dishes (Iwaki) were maintained at 37°C in DMEM F-12 without phenol red supplemented with 10% fetal calf serum and 20 mM 4-(2-hydroxyethyl)-1-piperazineethanesulfonic acid buffer. Images were acquired on a spinning-disk microscope (CSU22; Roper Scientific, Sarasota, FL) using a 491-nm laser and three band pass filters (510AF23, 590DF35, and 670DF40). Acquisitions were performed using oil immersion objectives mounted on a piezoelectric motor (Physik Instruments, Irvine, CA) and a QuantEM:512SC electron-multiplying CCD camera (Photometrics). The whole setup was driven with MetaMorph software (Molecular Devices, Sunnyvale, CA). After acquisition, images were scaled equivalently using MetaMorph software and converted to 8-bit images before being imported to Photoshop software (Adobe, Mountain View, CA).

For cell cycle studies, acquisitions were performed using a Plan-Apochromat 63×/1.4 oil objective lens. *Z*-stacks (10 planes 1 µm apart covering the entire nucleus) were acquired at 10-min intervals during ~20 h. For quantifications, the timing of disappearance and reappearance of foci was manually recorded on individual dividing cells. Box plots were then generated using KaleidaGraph (Synergy Software, Reading, PA): each box encloses 50% of the values obtained, centered on the median value. The bars extending from the top and bottom of each box mark the minimum and maximum values within the data set falling within an acceptable range. Values falling outside of this range are displayed as an individual point.

FRAP experiments on GFP-Nup107 and GFP-Nup43 cells were performed using a Plan-Apochromat 63×/1.4 (FRAP on nuclear bodies) or a Plan-Apochromat 40×/1.25 oil objective lens. For each cell, three prebleach images were taken, and either a single 10-pixel (2.4-µm) spot containing a nuclear body (along with three spots covering the NE in some cells) or a square region covering approximately half of the nucleus and part of the cytoplasm was bleached with the 473-nm line at 100% transmission (three iterations). *Z*-stacks (nine planes 1 µm apart covering the entire nuclei) were acquired at 10-s intervals for 12 frames and then at 1-min intervals for 30 frames.

Quantifications of fluorescence recovery were performed using the MetaMorph software on additive projections of one to three consecutive relevant *Z*-planes. When required, sequences were aligned using the "turboreg" registration plug-in on ImageJ (National Institutes of Health, Bethesda, MD). For each cell, the mean fluorescence intensities within circular regions of 8 pixels covering the bleached nuclear body (I) and (in the case of half-bleached nuclei) within intranuclear regions apparently devoid of nuclear bodies were measured at each time point. After background (BG) subtraction, the fluorescence signals were subjected to double normalization using a manually defined region (T) encompassing the whole nucleus (excluding the NE) to take into account the loss of total nuclear signal due to the bleach pulse and bleaching during postbleach imaging as previously described, $[(I_t - BG_t)/(I_{prebleach} - BG_{prebleach})]/[(T_t - BG_t)/(T_{prebleach} - BG_{prebleach})]$ (Phair *et al.*, 2004). These measurements were then normalized to 0 for the image taken immediately after photobleaching and to 1 for the steady-state distribution of fluorescence (mean of three images acquired just before photobleaching). The resulting graphs were generated using Excel (Microsoft).

The recovery curves for each cell were fitted to a monoexponential equation (also called reaction-dominant model, as described by Sprague *et al.*, 2004). In this reaction-dominant scenario, diffusion occurs so rapidly that it is not taken in account in the model. The corresponding molecules are thus considered to be part of a "freely" diffusing population.

## ACKNOWLEDGMENTS

We are grateful to M. Gillard and N. Renault for help with plasmid constructs; M. Matunis, D. Weil, F. Perez, J. Ellenberg, B. Burke, V. Cordes, B. Fontoura, D. Hernandez-Verdun, I. Mattaj, and R. Walczak for generously providing constructs, cell lines, or antibodies; and J. Beaudouin and members of our laboratories for valuable comments and critical reading of the manuscript. We acknowledge the ImagoSeine facility, member of the France BioImaging infrastructure

supported by the French National Research Agency (ANR-10-INSB-04, Investments of the Future). These studies were supported by the Centre National de la Recherche Scientifique, the Fondation ARC pour la Recherche sur le Cancer (Programme ARC; to V.D.), the Ministère de l'Enseignement Supérieur et de la Recherche (PhD fellowships to A.A.), and National Institutes of Health Grant RO1 GM-059975 to M.A.P.

## REFERENCES

Bai XT, Gu BW, Yin T, Niu C, Xi XD, Zhang J, Chen Z, Chen SJ (2006). Trans-repressive effect of NUP98-PMX1 on PMX1-regulated c-FOS gene through recruitment of histone deacetylase 1 by FG repeats. Cancer Res 66, 4584–4590.

Belgareh N, Rabut G, Bai SW, van Overbeek M, Beaudouin J, Daigle N, Zatsepina OV, Pasteau F, Labas V, Fromont-Racine M, *et al.* (2001). An evolutionarily conserved NPC subcomplex, which redistributes in part to kinetochores in mammalian cells. J Cell Biol 154, 1147–1160.

Bilokapic S, Schwartz TU (2013). Structural and functional studies of the 252 kDa nucleoporin ELYS reveal distinct roles for its three tethered domains. Structure 21, 572–580.

Blevins MB, Smith AM, Phillips EM, Powers MA (2003). Complex formation among the RNA export proteins Nup98, Rae1/Gle2, and TAP. J Biol Chem 278, 20979–20988.

Bodoor K, Shaikh S, Salina D, Raharjo WH, Bastos R, Lohka M, Burke B (1999). Sequential recruitment of NPC proteins to the nuclear periphery at the end of mitosis. J Cell Sci 112, 2253–2264.

Buckler-White AJ, Humphrey GW, Pigiet V (1980). Association of polyoma T antigen and DNA with the nuclear matrix from lytically infected 3T6 cells. Cell 22, 37–46.

Bui KH, von Appen A, DiGuilio AL, Ori A, Sparks L, Mackmull MT, Bock T, Hagen W, Andres-Pons A, Glavy JS, Beck M (2013). Integrated structural analysis of the human nuclear pore complex scaffold. Cell 155, 1233–1243.

Chakraborty P, Wang Y, Wei JH, van Deursen J, Yu H, Malureanu L, Dasso M, Forbes DJ, Levy DE, Seemann J, Fontoura BM (2008). Nucleoporin levels regulate cell cycle progression and phase-specific gene expression. Dev Cell 15, 657–667.

Chatel G, Desai SH, Mattheyses AL, Powers MA, Fahrenkrog B (2012). Domain topology of nucleoporin Nup98 within the nuclear pore complex. J Struct Biol 177, 81–89.

D'Angelo MA, Anderson DJ, Richard E, Hetzer MW (2006). Nuclear pores form de novo from both sides of the nuclear envelope. Science 312, 440–443.

D'Angelo MA, Raices M, Panowski SH, Hetzer MW (2009). Age-dependent deterioration of nuclear pore complexes causes a loss of nuclear integrity in postmitotic cells. Cell 136, 284–295.

Doucet CM, Talamas JA, Hetzer MW (2010). Cell cycle-dependent differences in nuclear pore complex assembly in metazoa. Cell 141, 1030–1041.

Enninga J, Levay A, Fontoura BM (2003). Sec13 shuttles between the nucleus and the cytoplasm and stably interacts with Nup96 at the nuclear pore complex. Mol Cell Biol 23, 7271–7284.

Ernoult-Lange M, Wilczynska A, Harper M, Aigueperse C, Dautry F, Kress M, Weil D (2009). Nucleocytoplasmic traffic of CPEB1 and accumulation in Crm1 nucleolar bodies. Mol Biol Cell 20, 176–187.

Floch AG, Palancade B, Doye V (2014). Fifty years of nuclear pores and nucleocytoplasmic transport studies: multiple tools revealing complex rules. Methods Cell Biol 122, 1–40.

Fontoura BM, Blobel G, Matunis MJ (1999). A conserved biogenesis pathway for nucleoporins: proteolytic processing of a 186-kilodalton precursor generates Nup98 and the novel nucleoporin, Nup96. J Cell Biol 144, 1097–1112.

Franks TM, Hetzer MW (2013). The role of Nup98 in transcription regulation in healthy and diseased cells. Trends Cell Biol 23, 112–117.

Fricker M, Hollinshead M, White N, Vaux D (1997). Interphase nuclei of many mammalian cell types contain deep, dynamic, tubular membrane-bound invaginations of the nuclear envelope. J Cell Biol 136, 531–544.

Gillespie PJ, Khoudoli GA, Stewart G, Swedlow JR, Blow JJ (2007). ELYS/MEL-28 chromatin association coordinates nuclear pore complex assembly and replication licensing. Curr Biol 17, 1657–1662.

Gonzalez-Aguilera C, Askjaer P (2012). Dissecting the NUP107 complex: multiple components and even more functions. Nucleus 3, 340–348.

Gough SM, Slape CI, Aplan PD (2011). NUP98 gene fusions and hematopoietic malignancies: common themes and new biologic insights. Blood 118, 6247–6257.

Griffis ER, Altan N, Lippincott-Schwartz J, Powers MA (2002). Nup98 is a mobile nucleoporin with transcription-dependent dynamics. Mol Biol Cell 13, 1282–1297.

Griffis ER, Xu S, Powers MA (2003). Nup98 localizes to both nuclear and cytoplasmic sides of the nuclear pore and binds to two distinct nucleoporin subcomplexes. Mol Biol Cell 14, 600–610.

Hendzel MJ, Wei Y, Mancini MA, Van Hooser A, Ranalli T, Brinkley BR, Bazett-Jones DP, Allis CD (1997). Mitosis-specific phosphorylation of histone H3 initiates primarily within pericentromeric heterochromatin during G2 and spreads in an ordered fashion coincident with mitotic chromosome condensation. Chromosoma 106, 348–360.

Hodel AE, Hodel MR, Griffis ER, Hennig KA, Ratner GA, Xu S, Powers MA (2002). The three-dimensional structure of the autoproteolytic, nuclear pore-targeting domain of the human nucleoporin Nup98. Mol Cell 10, 347–358.

Kasper LH, Brindle PK, Schnabel CA, Pritchard CE, Cleary ML, van Deursen JM (1999). CREB binding protein interacts with nucleoporin-specific FG repeats that activate transcription and mediate NUP98-HOXA9 oncogenicity. Mol Cell Biol 19, 764–776.

Landry JJ, Pyl PT, Rausch T, Zichner T, Tekkedil MM, Stutz AM, Jauch A, Aiyar RS, Pau G, Delhomme N, *et al.* (2013). The genomic and transcriptomic landscape of a HeLa cell line. G3 (Bethesda) 3, 1213–1224.

Laurell E, Beck K, Krupina K, Theerthagiri G, Bodenmiller B, Horvath P, Aebersold R, Antonin W, Kutay U (2011). Phosphorylation of Nup98 by multiple kinases is crucial for NPC disassembly during mitotic entry. Cell 144, 539–550.

Laurell E, Kutay U (2011). Dismantling the NPC permeability barrier at the onset of mitosis. Cell Cycle 10, 2243–2245.

Liang Y, Franks TM, Marchetto MC, Gage FH, Hetzer MW (2013). Dynamic association of NUP98 with the human genome. PLoS Genet 9, e1003308.

Light WH, Freaney J, Sood V, Thompson A, D'Urso A, Horvath CM, Brickner JH (2013). A conserved role for human Nup98 in altering chromatin structure and promoting epigenetic transcriptional memory. PLoS Biol 11, e1001524.

Lin CL, Evans V, Shen S, Xing Y, Richter JD (2010). The nuclear experience of CPEB: implications for RNA processing and translational control. RNA 16, 338–348.

Loiodice I, Alves A, Rabut G, Van Overbeek M, Ellenberg J, Sibarita JB, Doye V (2004). The entire Nup107–160 complex, including three new members, is targeted as one entity to kinetochores in mitosis. Mol Biol Cell 15, 3333–3344.

Mansfeld J, Guttinger S, Hawryluk-Gara LA, Pante N, Mall M, Galy V, Haselmann U, Muhlhausser P, Wozniak RW, Mattaj IW, *et al.* (2006). The conserved transmembrane nucleoporin NDC1 is required for nuclear pore complex assembly in vertebrate cells. Mol Cell 22, 93–103.

Mitchell JM, Mansfeld J, Capitanio J, Kutay U, Wozniak RW (2010). Pom121 links two essential subcomplexes of the nuclear pore complex core to the membrane. J Cell Biol 191, 505–521.

Oka M, Asally M, Yasuda Y, Ogawa Y, Tachibana T, Yoneda Y (2010). The mobile FG nucleoporin Nup98 is a cofactor for Crm1-dependent protein export. Mol Biol Cell 21, 1885–1896.

Phair RD, Gorski SA, Misteli T (2004). Measurement of dynamic protein binding to chromatin in vivo, using photobleaching microscopy. Methods Enzymol 375, 393–414.

Powers MA, Macaulay C, Masiarz FR, Forbes DJ (1995). Reconstituted nuclei depleted of a vertebrate GLFG nuclear pore protein, p97, import but are defective in nuclear growth and replication. J Cell Biol 128, 721–736.

Pritchard CE, Fornerod M, Kasper LH, van Deursen JM (1999). RAE1 is a shuttling mRNA export factor that binds to a GLEBS-like NUP98 motif at the nuclear pore complex through multiple domains. J Cell Biol 145, 237–254.

Rabut G, Doye V, Ellenberg J (2004). Mapping the dynamic organization of the nuclear pore complex inside single living cells. Nat Cell Biol 6, 1114–1121.

Radu A, Moore MS, Blobel G (1995). The peptide repeat domain of nucleoporin Nup98 functions as a docking site in transport across the nuclear pore complex. Cell 81, 215–222.

Rasala BA, Orjalo AV, Shen Z, Briggs S, Forbes DJ (2006). ELYS is a dual nucleoporin/kinetochore protein required for nuclear pore assembly and proper cell division. Proc Natl Acad Sci USA 103, 17801–17806.

Rasala BA, Ramos C, Harel A, Forbes DJ (2008). Capture of AT-rich chromatin by ELYS recruits POM121 and NDC1 to initiate nuclear pore assembly. Mol Biol Cell 19, 3982–3996.
Rosenblum JS, Blobel G (1999). Autoproteolysis in nucleoporin biogenesis. Proc Natl Acad Sci USA 96, 11370–11375.
Salsi V, Ferrari S, Gorello P, Fantini S, Chiavolelli F, Mecucci C, Zappavigna V (2014). NUP98 fusion oncoproteins promote aneuploidy by attenuating the mitotic spindle checkpoint. Cancer Res 74, 1079–1090.
Sarma NJ, Yaseen NR (2013). Dynein light chain 1 (DYNLT1) interacts with normal and oncogenic nucleoporins. PLoS One 8, e67032.
Savas JN, Toyama BH, Xu T, Yates JR 3rd, Hetzer MW (2012). Extremely long-lived nuclear pore proteins in the rat brain. Science 335, 942.
Savino TM, Bastos R, Jansen E, Hernandez-Verdun D (1999). The nucleolar antigen Nop52, the human homologue of the yeast ribosomal RNA processing RRP1, is recruited at late stages of nucleologenesis. J Cell Sci 112, 1889–1900.
Schmidt HB, Gorlich D (2015). Nup98 FG domains from diverse species spontaneously phase-separate into particles with nuclear pore-like permselectivity. Elife 4, e04251.
Schwartz M, Travesa A, Martell SW, Forbes DJ (2015). Analysis of the initiation of nuclear pore assembly by ectopically targeting nucleoporins to chromatin. Nucleus 6, 40–54.
Singer S, Zhao R, Barsotti AM, Ouwehand A, Fazollahi M, Coutavas E, Breuhahn K, Neumann O, Longerich T, Pusterla T, *et al*. (2012). Nuclear pore component Nup98 is a potential tumor suppressor and regulates posttranscriptional expression of select p53 target genes. Mol Cell 48, 799–810.
Sprague BL, Pego RL, Stavreva DA, McNally JG (2004). Analysis of binding reactions by fluorescence recovery after photobleaching. Biophys J 86, 3473–3495.
Terry LJ, Wente SR (2009). Flexible gates: dynamic topologies and functions for FG nucleoporins in nucleocytoplasmic transport. Eukaryot Cell 8, 1814–1827.
Vollmer B, Antonin W (2014). The diverse roles of the Nup93/Nic96 complex proteins - structural scaffolds of the nuclear pore complex with additional cellular functions. Biol Chem 395, 515–528.
Walde S, Kehlenbach RH (2010). The part and the whole: functions of nucleoporins in nucleocytoplasmic transport. Trends Cell Biol 20, 461–469.
Wente SR, Rout MP (2010). The nuclear pore complex and nuclear transport. Cold Spring Harb Perspect Biol 2, a000562.
Wozniak R, Burke B, Doye V (2010). Nuclear transport and the mitotic apparatus: an evolving relationship. Cell Mol Life Sci 67, 2215–2230.
Xu S, Powers MA (2010). Nup98-homeodomain fusions interact with endogenous Nup98 during interphase and localize to kinetochores and chromosome arms during mitosis. Mol Biol Cell 21, 1585–1596.
Xu S, Powers MA (2013). In vivo analysis of human nucleoporin repeat domain interactions. Mol Biol Cell 24, 1222–1231.